ORIGINAL PAPER

Towards extracellular Ca²⁺ sensing by MRI: synthesis and calcium-dependent ¹H and ¹⁷O relaxation studies of two novel bismacrocyclic Gd³⁺ complexes

Kirti Dhingra · Petra Fousková · Goran Angelovski · Martin E. Maier · Nikos K. Logothetis · Éva Tóth

Abstract Two new bismacrocyclic Gd³⁺ chelates containing a specific Ca²⁺ binding site were synthesized as potential MRI contrast agents for the detection of Ca²⁺ concentration changes at the millimolar level in the extracellular space. In the ligands, the Ca²⁺-sensitive BAPTA-bisamide central part is separated from the DO3A macrocycles either by an ethylene (L^1) or by a propylene (L^2) unit [H_4BAPTA is 1,2-bis(o-aminophenoxy)ethane-N,N,N',N'-tetraacetic acid; H_3DO$_3$A is 1,4,7,10-tetraaza-cyclododecane-1,4,7-triacetic acid]. The sensitivity of the Gd³⁺ complexes towards Ca²⁺ and Mg²⁺ was studied by ¹H relaxometric titrations. A maximum relaxivity increase of 15 and 10% was observed upon Ca²⁺ binding to Gd_2L^1 and Gd_2L^2, respectively, with a distinct selectivity of Gd_2L^1 towards Ca²⁺ compared with Mg²⁺. For Ca²⁺ binding, association constants of log K = 1.9 (Gd_2L^1) and log K = 2.7 (Gd_2L^2) were determined by relaxometry. Luminescence lifetime measurements and UV–vis spectrophotometry on the corresponding Eu³⁺ analogues proved that the complexes exist in the form of monohydrated and nonhydrated species; Ca²⁺ binding in the central part of the ligand induces the formation of the monohydrated state. The increasing hydration number accounts for the relaxivity increase observed on Ca²⁺ addition. A ¹H nuclear magnetic relaxation dispersion and ¹⁷O NMR study on Gd_2L^1 in the absence and in the presence of Ca²⁺ was performed to assess the microscopic parameters influencing relaxivity. On Ca²⁺ binding, the water exchange is slightly accelerated, which is likely related to the increased steric demand of the central part leading to a destabilization of the Ln–water binding interaction.

K. Dhingra · G. Angelovski · N. K. Logothetis (✉)
Max Planck Institute for Biological Cybernetics,
Tübingen, Germany
e-mail: nikos.logothetis@tuebingen.mpg.de

P. Fousková · É. Tóth (✉)
Centre de Biophysique Moléculaire,
CNRS, rue Charles Sadron,
45071 Orléans Cedex 2, France
e-mail: eva.jakabtoth@cnrs-orleans.fr

M. E. Maier
Institut für Organische Chemie,
Universität Tübingen,
Tübingen, Germany

N. K. Logothetis
Imaging Science and Biomedical Engineering,
University of Manchester,
Manchester, UK

Introduction

Magnetic resonance imaging (MRI) is one of the most versatile techniques in clinical and experimental in vivo imaging. It provides excellent three-dimensional spatial resolution down to the 10-μm range, whole body coverage and the opportunity to noninvasively measure additional physiological parameters [1]. Its sensitivity is, however, 2–6 orders of magnitude lower than that of optical imaging. This can be overcome by using appropriate MRI contrast agents. Nowadays, more than 30% of

MRI examinations benefit from the use of paramagnetic contrast agents [2]. By accelerating the longitudinal or transverse relaxation of water protons, they increase the signal-to-noise ratio, which, in turn, positively influences the image contrast. The currently used clinical contrast agents are mainly Gd^{3+} chelates, making use of the high magnetic moment (seven unpaired electrons) and slow electronic relaxation of this paramagnetic lanthanide ion [3, 4]. These contrast agents are, however, mostly non-specific and provide only anatomical information. Nowadays, there is an active search for new classes of contrast agents capable of reflecting a change in biological activity in their local environment. A new field, molecular imaging, is being developed, with the aim of in vivo visualization of molecular events. Any molecular imaging procedure requires an imaging probe that is specific for a given molecular event. Examples of such "smart" potential contrast agents, sensing variables like pH [5–7], partial oxygen pressure [8, 9], ion and metabolite concentration [10–14], or enzyme activity [15, 16] have been described in the literature. They function on the basis of the modulation of one or more microscopic parameters of the Gd^{3+} chelate determining relaxivity, induced by a change in the local environment of the agent. Among the variables that influence the relaxivity of a contrast agent, the most important are the applied magnetic field ($\boldsymbol{B}_0$), the number of water molecules directly bound to the paramagnetic center (q), their exchange rate (k_{ex}), the water proton–Gd^{3+} distance (r_{GdH}), the electron spin relaxation times (T_{1e}, T_{2e}), the rotational correlation time (τ_R), and the presence and the number of water molecules in the so-called second coordination sphere (q^{2nd}) [2, 4, 17, 18].

Calcium (Ca^{2+}) is one of the most important metal ions for life as it controls muscular contraction, neural cell communication, hormonal secretion, etc. [19]. In the brain, Ca^{2+} acts as an important second messenger [20]. Synaptic transmission depends on the entry of calcium ions at the presynaptic terminal to cause fusion and release of vesicles. Significant changes in Ca^{2+} concentration take place during neuronal activity [21]. Tracking the dynamics of Ca^{2+} concentration changes could thus contribute to the understanding of basic aspects of neuronal regulation or to highlight the abnormalities in the diseased state [22]. Optical imaging based on fluorescent dyes possessing a calcium-dependent response has been widely used at the cellular or cell population level [23]. However, the intrinsic depth limitations associated with optical imaging restrict these applications to superficial regions. In contrast to optical imaging, MRI has no depth penetration limits and could be more adapted for tracking Ca^{2+} changes. Li et al. [11, 24] have proposed a potential MRI contrast agent, GdDOPTA, whose relaxivity was reported to be

sensitive to Ca^{2+} concentration in the 0.1–10-μM range. The two macrocyclic subunits of the dimeric ligand DOPTA serve as lanthanide(III) ion chelators, while the $BAPTA^{4-}$ subunit bridging the macrocycles is known for its high selectivity towards Ca^{2+} [H_4BAPTA is 1,2-bis (o-aminophenoxy)ethane-N,N,N',N'-tetraacetic acid]. The mechanism proposed for the Ca^{2+}-dependent relaxivity change of GdDOPTA accounts for changes in the number of water molecules directly bound to the paramagnetic metal ion (q) upon Ca^{2+} binding to the $BAPTA^{4-}$ moiety. $BAPTA^{4-}$ was proposed a long time ago as a selective fluorescent indicator for Ca^{2+} [25]. It presents several advantages for biological Ca^{2+} detection by optical methods: integrated aromatic chromophore moiety and pH insensitivity of Ca^{2+} complexation thanks to the low values of the protonation constants (6.36 and 5.47, both below physiological pH). More recently, another calcium-sensitive MRI probe was proposed by Atanasijevic et al. [20]. It is based on superparamagnetic iron oxide nanoparticles and calmodulin. In this approach, calcium-dependent protein–protein interactions lead to particle clustering and consequent changes in transverse relaxivity. Similarly to GdDOPTA, this agent had calcium-response in the micromolar Ca^{2+} concentration range. It was therefore proposed to detect elevated intracellular Ca^{2+} levels, provided it is combined to a cellular delivery system.

With the objective of detecting *extracellular* Ca^{2+} concentration changes by MRI methods, we synthesized two novel potential bismacrocyclic MRI contrast agents (Structure 1). Two Gd^{3+}-loaded 1,4,7,10-tetraazacyclododecane-1,4,7-triacetic acid (DO3A) derived units were connected by a BAPTA-derived linker capable of Ca^{2+} binding. However, in comparison with $BAPTA^{4-}$, the Ca^{2+} binding moiety in the central part of the ligand was designed to have a reduced affinity towards Ca^{2+} in order to shift to higher Ca^{2+} concentrations the range where the probe is expected to have a relaxivity response. The conditional stability constant of GdDOPTA–Ca at physiological pH was reported to be $1.0 \times 10^6 \text{ M}^{-1}$ [11]. Similarly, the fluorescent Ca^{2+} indicators used in biological applications and based on $BAPTA^{4-}$ are adapted to assess the cytosolic free Ca^{2+} concentration in the micromolar range. In contrast, the extracellular concentration of Ca^{2+} is in the millimolar range. The relaxivity response of a probe with affinity of $K \sim 10^6$ M for Ca^{2+} would have already leveled off at the millimolar level. The $BAPTA^{4-}$ ligand was therefore modified by replacing two carboxylates by the less strong donor amide functions. As for the macrocyclic Gd^{3+} binding site, it was designed to respond to the presence of Ca^{2+} by modulation of the hydration number with consequent change in the relaxivity.

Ln₂L¹(n=1)
Ln₂L²(n=2)
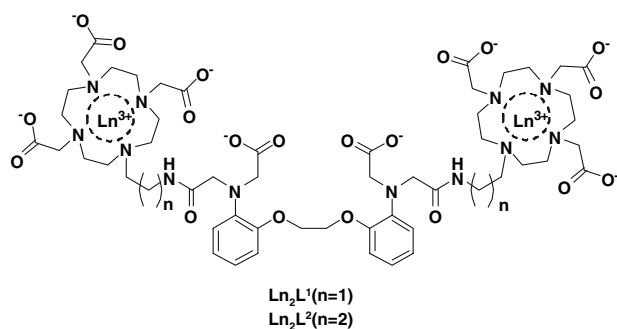
Structure 1

The proton relaxivities of the two new complexes were studied by relaxometric titrations at different Ca^{2+} concentrations and the relaxivity modulation by the Ca^{2+} concentration changes was confirmed. We specifically aimed to identify the microscopic factors responsible for the Ca^{2+}-dependent relaxivity response. To this end, a detailed mechanistic study was carried out. We used UV–vis absorption and luminescence lifetime measurements on the corresponding Eu^{3+} complexes to assess the number of inner-sphere water molecules and their variation on Ca^{2+} addition. The Gd_2L^1 complex was characterized by variable-temperature ^{17}O NMR spectroscopy and variable-field relaxivity measurements (nuclear magnetic relaxation dispersion, NMRD). The experimental data were evaluated on the basis of the Solomon–Bloembergen–Morgan theory, extended with a second-sphere contribution.

Experimental

Materials and methods

All chemicals were purchased at the purest grade commercially available and were used without further purification. Cyclen was purchased from Strem, France. Bromoethylamine hydrogen bromide, bromopropylamine hydrobromide, tert-butyl bromoacetate, N-methylpyrollidinone (dry), pyridine, H₄BAPTA, acetic anhydride and N,N-dimethylformamide (extra dry) were purchased from Sigma-Aldrich, Germany. Toluene, acetonitrile, dichloromethane and methanol were purchased as analytical grade solvents from Acros Organics, Germany. Lanthanide(III) chlorides were prepared by dissolving metal(III) oxides (Aldrich) in a slight excess of HCl (Carlo Erba, 37%) followed by evaporation of solvents and dissolution in H_2O.

High-performance liquid chromatography (HPLC) was performed at room temperature using a Varian (Australia) PrepStar instrument equipped with a PrepStar 335 photodiode array detector at 254 nm. Reversed-phase analytical

HPLC was performed in a stainless steel ChromSep (length 250 cm, internal diameter 4.6 mm, outside diameter 3/8 in. and particle size 8 µm) C18 column (Varian). The ligands were purified using the following gradient:

> Method A: 40% solvent A (methanol) and 60% solvent B (water) to 100% solvent B in 5 min running isocratically at 100% solvent B for 10 min and then to 60% solvent B in the next 2 min.
>
> Method B: 95% solvent A (acetonitrile, 0.1% HCOOH) and 5% solvent B (water, 0.1% HCOOH) to 70% solvent B in 10 min and then 100% in the next 8 min running isocratically for 12 min after that and then to 5% in next 2 min.

The flow rate used for analytical HPLC was 1 mL min⁻¹ and for preparative 65 mL min⁻¹. All solvents used were HPLC grade filtered through a 0.45-µm nylon-66 Millipore filter prior to use.

^1H and ^{13}C NMR spectra were recorded using a Bruker 400 MHz spectrometer (^1H—internal reference $CDCl_3$ at 7.27 ppm or D_2O at 4.75 ppm; ^{13}C—internal reference $CDCl_3$ at 77.0 ppm or tetramethylsilane at 0 ppm). All the experiments were performed at 298 K. Electrospray ionization (ESI) low-resolution mass spectrometry (LRMS) spectra were obtained using an SL 1100 system (Agilent, Germany) with ion-trap detection in positive and negative ion mode. IR spectra were recorded with a Nicolet Impact 400 D spectrometer using neat compounds as disks with KBr and only the major bands were noted. UV–vis spectra of $^5D_0 \leftarrow {}^7F_0$ transitions of Eu_2L^1 were obtained with a PerkinElmer Lambda 19 spectrometer in the region 577–581 nm with data steps of 0.05 nm [26]. The concentrations of the samples were approximately 0.02 M and the temperature dependence was measured in the interval 288–323 K in the absence and presence of Ca^{2+}. To maintain a constant temperature, thermostatizable cells with a 10-cm optical length were used. The luminescence measurements were performed with a Varian Eclipse spectrofluorimeter, equipped with a 450-W xenon arc lamp, a microsecond flash lamp and a red-sensitive photomultiplier (300–850 nm). The luminescence spectra were obtained after excitation of the $^5L_6 \leftarrow {}^7F_0$ band (394 nm). An aqueous solution (0.02 M) of Eu_2L^1 was measured at 298 K in the absence and presence of Ca^{2+}.

The ^1H NMRD profiles were recorded at the Laboratory of Inorganic and Bioinorganic Chemistry, Ecole Polytechnique Fédérale de Lausanne, Switzerland, using a Stelar Spinmaster FFC fast-field-cycling relaxometer covering magnetic fields from 2.35×10^{-4} to 0.47 T (proton Larmor frequency range 0.01–20 MHz). The temperature was controlled by a VTC90 temperature control unit and fixed by a gas flow. At higher fields, the relaxivity was recorded using Bruker Minispecs mq30 (30 MHz), mq40

(40 MHz) and mq60 (60 MHz), on a Bruker 4.7 T (200 MHz) cryomagnet connected to a Bruker Avance 200 console and with a Bruker Avance 500 spectrometer (500 MHz). The temperature was measured by a substitution technique [27] or via a preliminary calibration using methanol and ethylene glycol standards [28]. The longitudinal ($1/T_1$) and transverse ($1/T_2$) ^{17}O NMR relaxation rates were measured in the temperature range 277–344 K. The data were recorded using a Bruker Avance 500 (11.75 T, 67.8 MHz) spectrometer. The temperature was calculated according to a previous calibration with ethylene glycol and methanol [28]. The samples were measured in 5-mm NMR tubes and were enriched with *tert*-butanol to allow for the bulk magnetic susceptibility correction [29]. The $1/T_1$ data were obtained by the inversion recovery method, while the $1/T_2$ data were measured by the Carr–Purcell–Meiboom–Gill spin-echo technique. Acidified water ($HClO_4$, pH 3.8) was used as an external reference. Analyses of the ^{17}O NMR and ^1H NMRD experimental data were performed with the Visualiseur/Optimiseur programs running on a MATLAB platform version 6.5 [30, 31].

Synthesis

Compound **4a** was synthesized according to a previously reported procedure [32]. With use of an analogous method, compound **4b** was synthesized via **3b** from the substrate **1b** [33].

Compound **3b**. ^1H NMR (CDCl$_3$, 400 MHz), δ (ppm): 6.97–6.84 (m, 5H), 4.65 (s, 2H), 2.98–2.89 (m, 2H), 2.86–2.70 (m, 5H), 2.70–2.60 (m, 3H), 2.58–2.17 (m, 7H), 2.16–1.75 (m, 9H), 1.32 (br s, 2H), 1.06–1.03 (m, 27H). ^{13}C NMR 172.2, 171.2, 155.2, 152.9, 135.6, 127.1, 126.4, 81.3, 81.0, 65.7, 64.7, 55.4, 50.3, 48.9, 38.5, 37.8, 28.2, 26.7, 26.5, 25.2. ESI–MS *m/z*: [M + H]$^+$ calcd for $C_{37}H_{63}N_5O_8$, 705.5; found, 706.5.

Compound **4b**. ^1H NMR (CDCl$_3$, 400 MHz), δ (ppm): 8.19 (br s, 2H), 3.42–2.99 (m, 8H), 2.85–2.20 (m, 16H), 1.61 (br s, 2H), 1.41 (s, 27H). ^{13}C NMR (CDCl$_3$, 100 MHz), δ (ppm): 172.0, 169.8, 81.8, 81.1, 57.2, 55.9, 50.1, 49.4, 48.9, 38.5, 27.2, 27.1, 22.9. ESI–MS *m/z*: [M + H]$^+$ calcd for $C_{29}H_{57}N_5O_6$, 571.4; found, 572.4 .

General method for the synthesis of compounds 6a and 6b

Compound **4a** or **4b** (2 mmol) was dissolved in 5 mL of dry *N*-methylpyrollidinone with 50 µL of dry Et$_3$N and heated at 333 K for 15 min. Anhydride **5** [34] was then added to this reaction mixture (295 mg, 0.67 mmol) in small lots under N$_2$. After complete addition of **5**, the

solution was kept under continuous stirring at 333 K overnight. It was then evaporated, dissolved in dichloromethane and extracted with water. The organic layer was collected and evaporated to get a yellow oil. The crude product was then purified by reversed-phase HPLC using method A to get a light yellow fluffy solid.

1,2-Bis{[2-{[({1-[1,4,7-tris(*tert*-butoxycarbonylmethyl)-1,4,7,10-tetraazacyclododecane-10-yl]eth-2-yl}amino)carbonyl]methyl}-(carboxymethyl)amino]phenoxy}ethane, **6a**. Yield: 573 mg (55%) ^1H NMR (CDCl$_3$, 400 MHz), δ (ppm): 7.01–6.98 (m, 2H), 6.92–6.89 (m, 2H), 6.77–6.74 (m, 4H), 4.56 (d, *J* = 6.4 Hz, 2H, CH*H*O), 4.34 (d, *J* = 15.5 Hz, 2H, CH*H*CONH), 4.01 (d, *J* = 17.8 Hz, 2H, CH*H*COOH), 3.91 (d, *J* = 6.4 Hz, 2H, C*H*HO), 3.48 (d, *J* = 17.8 Hz, 2H, CH*H*COOH), 3.36–3.21 (m, 22H), 3.08–2.80 (m, 12H), 2.78–2.69 (m, 6H), 2.76–2.56 (m, 18H), 1.47 (s, 36H), 1.43 (s, 18H). ^{13}C NMR (CDCl$_3$, 100 MHz), δ (ppm): 175.2 (*C*ONH), 175.0 (*C*ONH), 170.2, 170.1, 149.4, 139.2, 120.6, 119.5, 115.4, 112.1, 81.8, 81.5, 66.4 (*C*H$_2$O), 60.7 (N*C*H$_2$CONH), 58.5 (*C*H$_2$COOH), 56.5, 54.8, 53.5, 51.3, 50.3, 49.7, 47.8, 32.1 (*C*H$_2$CH$_2$CONH), 29.6, 28.1. ESI–MS *m/z*: [M + H]$^+$ calcd for $C_{78}H_{130}N_{12}O_{20}$, 1,554.9; found, 1,555.9.

1,2-Bis{[3-{[({1-[1,4,7-tris(*tert*-butoxycarbonylmethyl)-1,4,7,10-tetraazacyclododecane-10-yl]prop-3-yl}amino)carbonyl]methyl}-(carboxymethyl)amino]phenoxy}ethane, **6b**. Yield: 424 mg (40%). ^1H NMR (CDCl$_3$, 400 MHz), δ (ppm): 7.08–7.06 (m, 2H), 6.91–6.89 (m, 2H), 6.85–6.82 (m, 4H), 4.49 (br s, 2H), 4.31 (br s, 4H), 4.08–3.73 (m, 8H), 3.57–3.09 (m, 20H), 3.04–2.47 (m, 32H), 2.40 (br s, 4H), 2.01 (br s, 2H), 1.53 (s, 18H), 1.48 (s, 36H). ^{13}C NMR (CDCl$_3$, 100 MHz), δ (ppm): 175.7, 173.4, 170.9, 170.2, 150.2, 139.8, 120.3, 120.2, 115.7, 112.2, 82.2, 82.0, 66.6, 61.0, 58.7, 56.5, 55.3, 49.6, 49.1, 47.6, 35.5, 28.6, 28.4, 22.2. ESI–MS *m/z*: [M + H]$^+$ calcd for $C_{80}H_{134}N_{12}O_{20}$, 1,582.9; found, 1,584.0.

General method for the synthesis of L¹ and L²

Neat trifluoroacetic acid (70 mL) was added to the previously obtained compound **6a** or **6b** (0.32 mmol) and the reaction was kept at room temperature for 24 h. Trifluoroacetic acid was then evaporated, and the residue was dried under vacuum and purified by reversed-phase HPLC using method B.

1,2-Bis{[2-{[({1-[1,4,7-tris(carboxymethyl)-1,4,7,10-tetraazacyclododecane-10-yl]eth-2-yl}amino)carbonyl]methyl}-(carboxymethyl)amino]phenoxy}ethane, **L¹**. Yield: 220 mg (60%). ^1H NMR (CDCl$_3$, 400 MHz), δ (ppm): 7.06–6.99 (m, 4H), 6.94 (t, *J* = 7.0 Hz, 2H), 6.87–6.85 (m, 2H), 4.27 (s, 4H), 3.83 (s, 4H), 3.77 (s, 4H), 3.58 (br s, 8H), 3.45 (s, 4H), 3.28–3.12 (m, 24H), 3.02–2.97 (m, 4H),

2.82–2.75 (m, 12H). ^{13}C NMR (D$_2$O, 100 MHz), δ (ppm): 177.6, 174.7, 170.5, 169.9, 150.1, 138.9, 122.5, 121.4, 117.4, 113.0, 67.0, 57.9, 56.7, 56.1, 55.3, 51.0, 50.6, 50.5, 49.2, 47.6, 33.5. IR (cm^{-1}): 3,426 (vs), 2,964 (m), 2,929 (m), 2,860 (m), 1,718 (s), 1,637 (vs), 1,384 (s), 1,355 (s), 1,328 (m), 1,240 (s), 1,203 (s), 762 (m), 694 (m). ESI–MS m/z: [M–H]$^-$ calcd for C$_{54}$H$_{82}$N$_{12}$O$_{20}$, 1,218.57; found, 1,217.7.

1,2-Bis{[3-{[({1-[1,4,7-tris(carboxymethyl)-1,4,7,10-tetraazacyclododecane-10-yl]prop-3-yl}amino)carbonyl]methyl}-(carboxymethyl)amino]phenoxy}ethane, L^2. Yield: 126 mg from 400 mg of **6b** (40%). 1H NMR (D$_2$O, 400 MHz), δ (ppm): 6.98–6.91 (m, 4H), 6.88 (t, J = 7.4, 2H), 6.82–6.80 (m, 2H), 4.20 (s, 4H), 3.78 (s, 4H), 3.74 (s, 4H), 3.57 (s, 4H), 3.39–3.31 (m, 8H), 3.27–3.20 (m, 8H), 3.13–2.92 (m, 20H), 2.89–2.83 (m, 8H), 2.65 (br s, 4H), 1.61–1.53 (m, 4H). ^{13}C NMR (D$_2$O, 100 MHz), δ (ppm): 177.7, 174.4, 149.9, 138.5, 122.3, 121.5, 117.4, 113.2, 67.1, 57.6, 56.2, 56.1, 55.4, 50.9, 50.5, 49.6, 49.2, 36.4, 22.6. ESI–MS m/z: [M–H]$^-$ calcd for C$_{56}$H$_{86}$N$_{12}$O$_{20}$, 1,246.6; found, 1,245.6.

Preparation of solutions of lanthanide(III) complexes

The complexes used for ^{1}H and ^{17}O relaxometric and UV–vis measurements were prepared by mixing a slight excess (5%) of the ligand solution with the appropriate lanthanide(III) chloride solution. The pH was adjusted to 7 using KOH solution and the reaction mixture was stirred at 323 K overnight. The absence of free Ln^{3+} was checked by xylenol orange indicator in HCl/urotropine buffer (pH 5.8). For each Gd$_2$L sample, the Gd^{3+} concentration was determined by measuring the bulk magnetic susceptibility shifts [35].

Gd$_2$L^1. ESI–LRMS m/z: [M–H + Na]$^-$ calcd for C$_{78}$H$_{124}$Gd$_2$N$_{12}$O$_{20}$, 1,525.1; found, 1,547.6. IR: 3,448 (vs), 1,602 (vs), 1,560 (s), 1,400 (m), 1,323 (m), 1,242 (m), 1,203 (vs), 1,085 (m), 762 (m), 723(m).

Eu$_2$L^1. ESI–LRMS m/z: [M–H]$^-$ calcd for C$_{54}$H$_{76}$Eu$_2$N$_{12}$O$_{20}$, 1,156.4; found 1,155.5.

Gd$_2$L^2. ESI–LRMS m/z: [M + H]$^+$ calcd for C$_{56}$H$_{80}$Gd$_2$N$_{20}$O$_{12}$, 1,553.1; found, 1,553.6.

Relaxometric Ca^{2+} titrations of Gd$_2$L^1 and Gd$_2$L^2

The titrations were performed at 11.75 T, 298 K and pH 7.3 [maintained by N-(2-hydroxyethyl)piperazine-N'-ethanesulfonic acid buffer]. A solution of CaCl$_2$ of known concentration was added stepwise to the complex solution and the longitudinal proton relaxation time T_1 was measured after each Ca^{2+} addition. The initial Gd^{3+} concentrations

were 7.4 and 4.0 mM for Gd$_2$L^1 and Gd$_2$L^2, respectively. The relaxivity r_1 was calculated from Eq. 1, using the actual Gd^{3+} concentration at each point of the titration:

$$\frac{1}{T_{1,\text{obs}}} = \frac{1}{T_{1,\text{d}}} + r_1[\text{Gd}], \tag{1}$$

where $T_{1,\text{obs}}$ is the observed longitudinal relaxation time, $T_{1,\text{d}}$ is its diamagnetic contribution in the absence of the paramagnetic substance and [Gd] is the concentration of Gd^{3+}.

Relaxometric Mg^{2+} titration of Gd$_2$L^1

The titration was done analogously to the Ca^{2+} titration (B = 11.75 T, 298 K; initial Gd^{3+} concentration of 2.6 mM). When the Mg^{2+}-to-complex ratio was 23 (in the Ca^{2+} titration, the plateau was already reached at this Ca^{2+}-to-Gd$_2$L^1 ratio), a Ca^{2+} solution was added stepwise and the relaxivity was measured.

Results and discussion

Synthesis of ligands

The ligands were prepared from the appropriate anhydride and amine precursors in a facile two-step procedure as shown in Scheme 1. Compounds **1a**, **1b**, **2** and **5** were synthesized according to reported procedures [32–34]. Protected amines **3a** an **3b** were synthesized by alkylating **2** with **1a** or **1b** in acetonitrile. Hydrogenation of the resulting products in methanol using 10% Pd on carbon as a catalyst yielded **4a** and **4b**. Bismacrocycles **6a** and **6b** were obtained by coupling of amines **4a** or **4b** to an anhydride **5** in N-methylpyrrolidinone and triethylamine. After the purification, they were hydrolyzed with neat trifluoroacetic acid and purified by reversed-phase HPLC giving the final ligands L^1 and L^2. It is interesting to note that an additional proof for the extremely high steric constraints in the bismacrocyclic systems studied was observed in 2D NMR (correlation spectroscopy, heteronuclear single quantum coherence) spectra of **6a** (Figs. S13, S14). The splitting of the signals occurs on all methylene groups not belonging to the macrocyclic ring; this disappears upon the removal of *tert*-butyl protective groups in L^1.

Relaxometric Ca^{2+} titrations of Gd$_2$L^1 and Gd$_2$L^2

The titration curves are represented as the variation of the relaxivity of the Gd^{3+} complex solution versus the Ca^{2+} concentration (Fig. 1). The maximum relaxivity increase

Scheme 1 Synthesis of the ligands and their lanthanide(III) complexes. Reagents and conditions: *a* benzyl chloroformate, K₂CO₃, water/dioxane; *b tert*-butylbromoacetate, NaHCO₃, MeCN, 70%; *c* **1a** or **1b**, K₂CO₃, MeCN, 60%; *d* H₂, Pd/C, MeOH; *e* Ac₂O, pyridine, 75%; *f* N-methylpyrollidinone, Et₃N; *g* trifluoroacetic acid; *h* LnCl₃·6H₂O
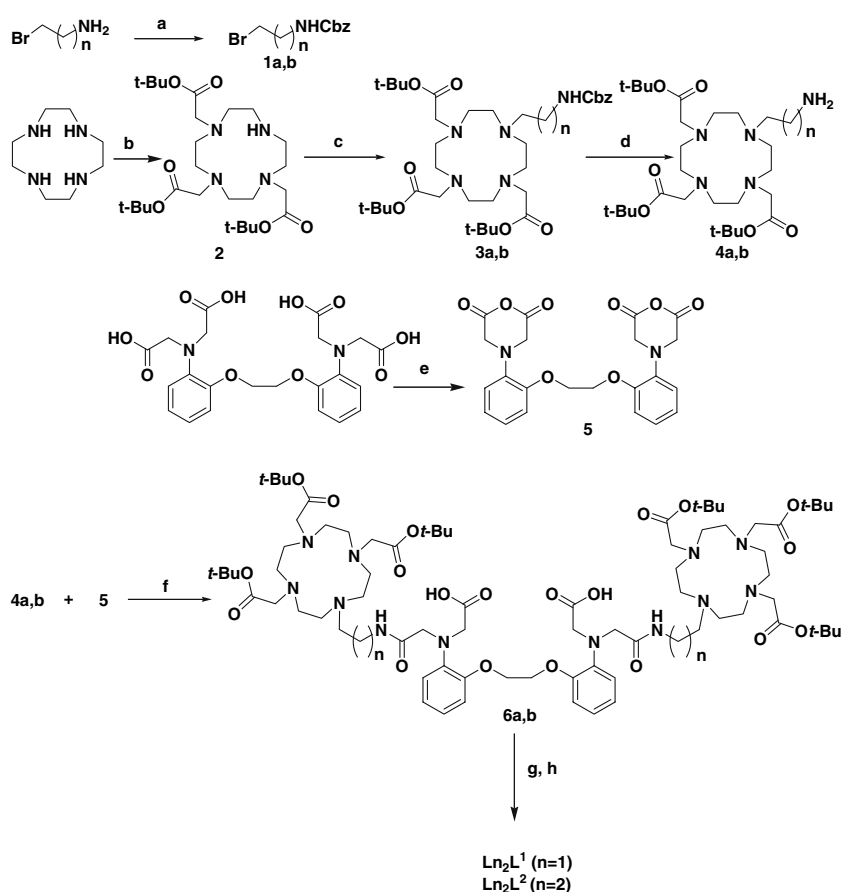
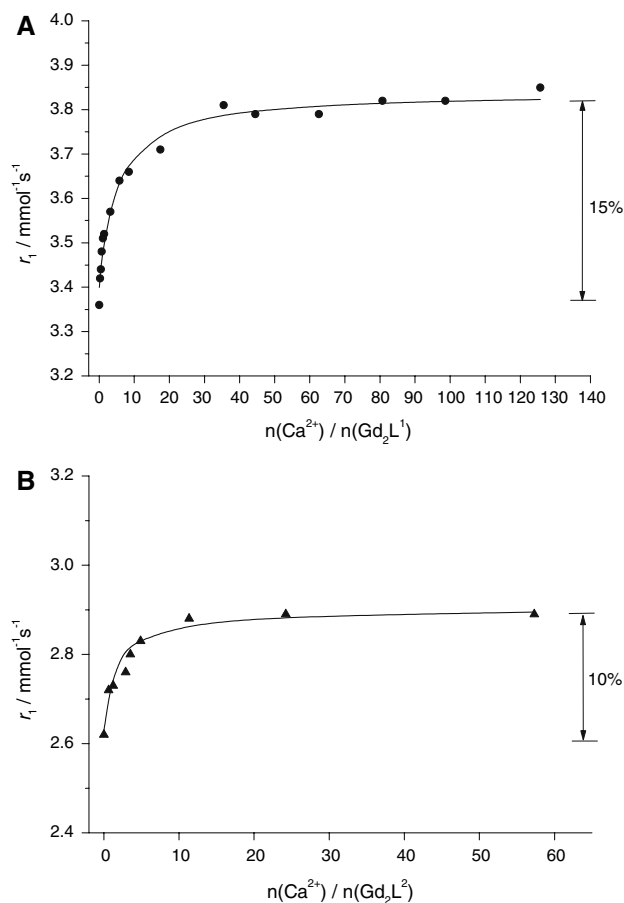upon Ca^{2+} addition was 15% for Gd_2L^1 and 10% for Gd_2L^2. The saturation of both curves occurs at relatively high Ca^{2+} concentrations (approximately 20 equiv of Ca^{2+} for Gd_2L^1 and approximately 5 equiv of Ca^{2+} for Gd_2L^2). The titration curves were fitted to obtain the apparent association constants, which are log $K = 1.9 \pm 0.2$ and log $K = 2.7 \pm 0.2$ for Gd_2L^1 and Gd_2L^2, respectively. Similarly to the case for previously investigated BAPTA-type complexes [11, 25], 1:1 binding stoichiometry has been assumed. These association constants are to be compared with the conditional stability constant, log $K_{cond} = 6.9$ of $CaBAPTA^{2-}$ at pH 7.0, calculated by taking into account the protonation constants of $BAPTA^{4-}$ [25]. The constants obtained for our systems are 3–4 orders of magnitude lower. This difference can be rationalized by the fact that even on Ca^{2+} binding, the amide groups of the ligand remain coordinated to the lanthanide as indicated by proton relaxivity and luminescence data on the Gd^{3+} and Eu^{3+} complexes, respectively (see below). Therefore, in comparison with $CaBAPTA^{2-}$, there are two carboxylate donors fewer coordinating to the Ca^{2+} ion, which is responsible for the considerably reduced stability. It is interesting to note that the stability of the Gd_2L^2–Ca complex is somewhat higher than that of Gd_2L^1–Ca. This is likely related to the higher flexibility of the Ca^{2+} binding

site in Gd_2L^2–Ca, where the propylene linker between the macrocycle and the Ca^{2+} binding site induces fewer steric constraints, hence ensuring a better "overwrapping" of the cation by the chelator. We have to note that for GdDOP-TA-Ca, possessing an integral $BAPTA^{4-}$ unit for Ca^{2+} binding, Li et al. [11] reported a much higher apparent association constant, $K = 1.0 \times 10^6$ M.

Relaxometric Mg^{2+} titration of Gd_2L^1

The relaxivity remains approximately constant upon addition of Mg^{2+}, then it increases upon Ca^{2+} addition even in the presence of a large amount of Mg^{2+} (Fig. 2). The relaxivity increase after Ca^{2+} addition (16%) was similar to that observed in the Ca^{2+} titration without the presence of Mg^{2+}. The insensitivity of Gd_2L^1 towards Mg^{2+} is due to the lower stability of BAPTA-derived complexes with Mg^{2+} compared with Ca^{2+}. The titration curve shows that, though the affinity of our chelator for Ca^{2+} is diminished in comparison with $BAPTA^{4-}$, the selectivity versus Mg^{2+} is conserved. The discrimination of BAPTA-type ligands towards Ca^{2+} compared with Mg^{2+} is supposed to stem from the right size of the binding cavity for the larger-sized Ca^{2+}, which is already too big for Mg^{2+} and cannot
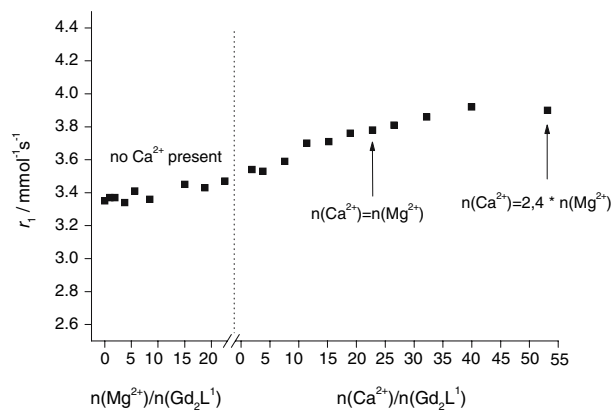
Fig. 1 Relaxometric Ca^{2+} titration curves of Gd_2L^1 (a) and Gd_2L^2 (b) obtained at 298 K and 11.75 T. The *lines* correspond to the fit as explained in the text

Fig. 2 Relaxometric titration curve of Gd_2L^1 with Mg^{2+} followed by addition of Ca^{2+} (298 K, 11.75 T)

$$q = A'(\Delta k_{H_2O} - k_{D_2O})_{corr}, \qquad (2)$$

where A' is 1.2 ms and the correction factor for the contribution of the second sphere is –0.25 m s^{-1}. The longitudinal ^{17}O and ^1H relaxation rates (vide supra) indicate that we cannot neglect the effect of second-sphere water molecules. The noninteger hydration number suggests the presence of both $q = 1$ and $q = 0$ species. Upon the addition of Ca^{2+} to the Eu^{3+} complex, the hydration number determined by luminescence increases to $q \approx 0.7$ ($\tau_{H_2O} = 0.422$ ms and $\tau_{D_2O} = 0.661$ ms) (Fig. 3). Such an increase of q can be interpreted in terms of a shift towards the monohydrated species.

To investigate further the hydration state, variable-temperature UV–vis measurements were performed on Eu_2L^1. In general, the presence of a hydration equilibrium of europium(III) species leads to the appearance of two absorption bands for the $^5D_0 \leftarrow {}^7F_0$ transition with peak separations of more than 0.5 nm [39, 40]. High-resolution UV–vis absorption spectra of a Eu_2L^1 aqueous solution (pH 7) were recorded in the 577–581-nm region at various temperatures and Ca^{2+} concentrations. The measurements revealed two temperature-invariant absorption bands, which could be deconvoluted into two symmetrical peaks (Fig. 4). The separation of those peaks is about 0.5 nm and lies in the range typical of different coordination environments of Eu^{3+} [41, 42]. We assume that in the absence of Ca^{2+}, there are two nine-coordinate species present; in both species the amines and carboxylates of the macrocycle as well as the amide oxygen are coordinated to the lanthanide, and either carboxylate from the central part or one water molecule completes the coordination sphere to a coordination number of nine, which is the usual coordination number for this type of Ln^{3+} complex (Fig. 5). The coordination of amide oxygens is supported by IR measurements performed on the ligand L^1 and its Gd^{3+} complex: the comparison of the two IR spectra (Figs. S5, S6) shows that the amide

constrict further to envelop snugly this smaller cation (the association constant of MgBAPTA^{2-} is log K = 1.8) [25]. Spectrophotometric measurements on the Mg^{2+}–BAPTA system proved that Mg^{2+} coordination affects only half of the ligand, in contrast to Ca^{2+} coordination, where the entire ligand is involved [25].

Luminescence and UV–vis absorption studies to assess the hydration state of Eu_2L^1

In order to determine the number of water molecules coordinated to the lanthanide ion before and after Ca^{2+} binding to the complex, we performed luminescence lifetime measurements on Eu_2L^1 in H_2O and D_2O solutions [36–38]. In the absence of Ca^{2+}, the luminescence lifetimes are $\tau_{H_2O} = 0.328$ ms and $\tau_{D_2O} = 0.408$ ms. The hydration number, $q = 0.4$, was calculated according to the revised equation of Beeby et al. [38] which involves a correction for the contribution of second-sphere water molecules (Eq. 2):
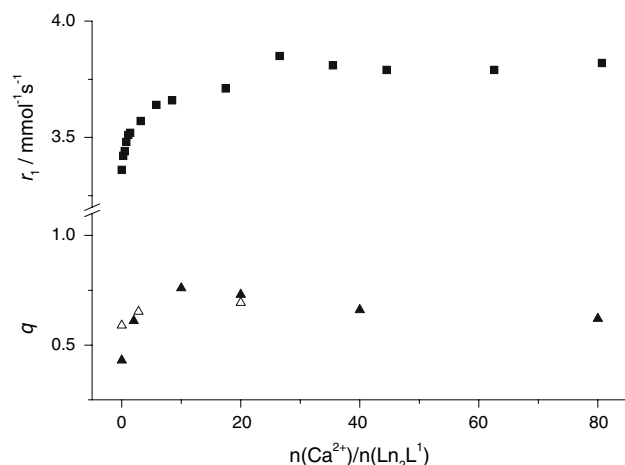
Fig. 3 Dependence of the relaxivity r_1 and of the hydration number q on the Ca^{2+}-to-complex ratio for Ln_2L^1. *Squares* correspond to the relaxivity values obtained from the relaxometric titration of Gd_2L^1 (298 K, 11.75 T). *Filled triangles* represent the hydration number obtained from luminescence lifetime studies on Eu_2L^1 and *open triangles* correspond to the molar fraction of the monohydrated species determined for Eu_2L^1 by UV–vis spectroscopy (ratio of the integrals of the absorption bands corresponding to monohydrated and nonhydrated complex; see text)

absorption is affected by complexation to the lanthanide ion.

Among analogous structures, lanthanide complexes of monomeric DO3A derivatives bearing $–(CH_2)_n–NHCO–R$ ($n = 2, 3$) amide units have been reported in the literature [43]. With Eu^{3+} and Gd^{3+}, the $n = 2$ ligand forms monohydrated complexes, while the $n = 3$ ligand forms nonhydrated complexes. In contrast to this, Eu_2L^1 contains a carboxylate in the central part as a potential donor which can partially replace the water molecule in the inner coordination sphere. This leads to the presence of the two
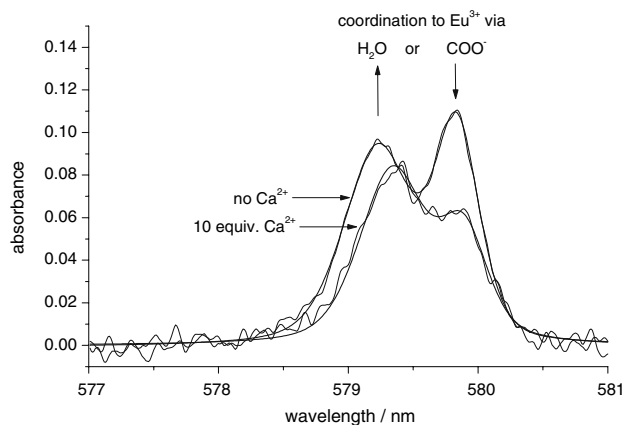
Fig. 4 Experimental and fitted UV–vis spectra (323 K, pH 7) of Eu_2L^1 in the absence and presence of Ca^{2+}. On addition of Ca^{2+}, the relative intensity of the band at lower wavelength increases, while that of the band at higher wavelength decreases
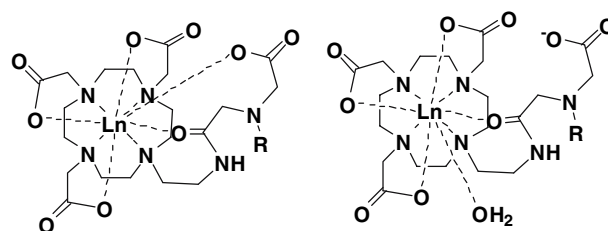
Fig. 5 Proposed structures present in aqueous solution of Ln_2L^1. R stands for the remaining part of the bismacrocyclic complex

structures as proposed in Fig. 5, and consequently to a reduced hydration number.

Upon Ca^{2+} addition to a Eu_2L^1 solution, the relative intensity of the two UV–vis absorption bands changes: the band at higher wavelengths decreases, while the other band increases (Fig. 4) [44]. In parallel, the luminescence measurements indicate an increase of the hydration number. Therefore, we conclude that the band which decreases in intensity (at 579.9 nm) on Ca^{2+} addition can be attributed to the $q = 0$ complex, while the band which increases in intensity (579.3 nm) can be attributed to the monohydrated complex. We assume that both in the presence and in the absence of Ca^{2+}, the amide oxygen remains coordinated to the lanthanide ion to preserve the overall coordination number of nine. If the amide oxygen participated also in the Ca^{2+} coordination, the concomitant increase in the hydration number and in relaxivity would be more prominent than what is experimentally observed. The Ca^{2+} binding in the central part of the complex demands the coordination of the central carboxylates, which, by leaving the coordination environment of Ln^{3+}, allow a water molecule to bind to the lanthanide ion. Therefore, the Ca^{2+} binding in the central part will favor the formation of the monohydrated complex (Fig. 5).

Relation between the Ca^{2+}-dependent hydration number q and relaxivity

Upon stepwise addition of Ca^{2+}, we observe a good correlation between the relaxivity increase of the Gd_2L^1 complex and the increase in q determined from the luminescence lifetime measurements on the Eu^{3+} analogue (Fig. 3). In addition, we also calculated the ratio of the integrals of the two UV–vis absorption bands (attributed to $q = 0$ and $q = 1$) of Eu_2L^1 at various Ca^{2+} concentrations. The q values obtained in this way overlap with those measured by luminescence. This supports our hypothesis that the complex Ln_2L^1 exists in the form of two differently hydrated species, each with an overall coordination number of nine. As was proved by the UV–vis studies, their ratio is temperature-independent but it shifts towards the monohydrated species

with increasing Ca^{2+} concentration, resulting in a relaxivity increase.

The relaxivity of the Gd_2L^2 complex is lower than that of the L^1 analogue, which suggests that q is also lower. In the case of the monomeric DO3A derivatives bearing –$(CH_2)_n$–NHCO–R amide units, with the propyl-linked ($n = 3$) amide $q = 0$ was determined for the Eu^{3+} and Gd^{3+} complexes [43]. The extra steric demand associated with the enlargement of the chelate ring incorporating the amide carbonyl group was found to be sufficient to suppress water coordination. For Gd_2L^2, the relaxivities suggest $q > 0$. Moreover, the relaxivity increases on Ca^{2+} addition, though to a smaller extent than for Gd_2L^1. Therefore, we assume that two differently hydrated species exist also for Ln_2L^2 complexes, with an increased proportion of the nonhydrated species compared with Ln_2L^1. The relaxivity change observed on Ca^{2+} addition indicates that the central carboxylate participates in the lanthanide coordination; on Ca^{2+} binding this carboxylate is removed from the lanthanide ion and replaced by a water molecule. The small relaxivity change shows that the participation of this carboxylate in the lanthanide coordination is limited with respect to Gd_2L^1.

For GdDOPTA, Li et al. [11, 24] reported a more important variation of q and a correspondingly greater relaxivity change on Ca^{2+} binding. This is likely related to the more flexible nature of the central $BAPTA^{4-}$ part of the DOPTA ligand in contrast to the BAPTA-bisamide moiety in our case, where the monoamide functionalities are integrated in the central skeleton of the ligand and have much less flexibility to change coordination from Gd^{3+} to Ca^{2+}.

^{1}H and ^{17}O relaxation studies of Gd_2L^1: evaluation of the parameters influencing proton relaxivity

^{1}H NMRD profiles were recorded for Gd_2L^1 with and without Ca^{2+}. In the presence of Ca^{2+}, an increase in the relaxivity was observed at all frequencies, related to an increase in the hydration number. The relaxivity at 20 MHz and 298 K in the absence and presence of Ca^{2+} is 5.74 and 6.13 mM^{-1} s^{-1}, respectively, slightly higher than the relaxivites of currently used MRI contrast agents [2, 4, 19, 45].

The transverse ^{17}O relaxation rates indicate a relatively slow water exchange (Fig. 6), which is visible from the curve of $\ln(1/T_{2r})$ versus inverse temperature: at low temperatures, $1/T_{2r}$ decreases with decreasing temperature. The reduced chemical shifts ($\Delta\omega_r$) in the absence of Ca^{2+} are smaller than would be expected for a $q = 0.4$ complex. Such small chemical shifts have previously been observed in systems with a significant second-sphere contribution

[46]. Therefore, the chemical shifts were not included in the final fitting. For the Ca^{2+}-free system, the transverse and longitudinal ^{17}O relaxation rates and the ^{1}H NMRD data were analyzed simultaneously (Fig. 6) on the basis of the Solomon–Bloembergen–Morgan approach, extended by a second-sphere contribution [46, 47]. The presence of free carboxylates in the complex induces a second-sphere contribution that affects both ^{1}H and ^{17}O longitudinal relaxation. In fact, by fitting the ^{17}O $1/T_1$ values without second-sphere contribution, we obtained inconceivably high rotational correlation times. The inner-sphere hydration number q was fixed to 0.4, the value found by luminescence measurements on Eu_2L^1. Since Eu^{3+} and Gd^{3+} have similar ionic radii, we expect a similar hydration mode for Gd_2L^1. To describe the second-sphere contribution, one water molecule per Gd^{3+} ($q^{2nd} = 1$) was considered during the fitting. The distance between the Gd^{3+} ion and the second-sphere water proton and oxygen was fixed to $r_{Gd-H}^{2nd} = 3.5$ Å and $r_{Gd-O}^{2nd} = 4.1$ Å, respectively, the enthalpy of activation to $\Delta H^{\#2nd} = 35$ kJ mol^{-1}, and the second-sphere water residence time to $\tau_m^{2nd} = 50$ ps [46, 47]. Other parameters were also fixed during the fitting in order to add some constraints. They are as follows: the hyperfine coupling constant, $A/\hbar = -3.8$ MHz; the distance between Gd^{3+} and the oxygen and the proton of the first-sphere water molecule, $r_{GdO} = 2.5$ Å and $r_{GdH} = 3.1$ Å, respectively. The distance of the closest approach of outer-sphere water molecules to Gd^{3+}, a, was fixed to 3.6 Å. The quadrupolar coupling constant $[\chi(1 + \eta^2/3)^{1/2}]$ was set to 7.58 MHz, the value of pure water. The activation energy E_v had to be fixed to 1 kJ mol^{-1}, otherwise the fit converged to negative values. In the fitting procedure, we used a model which considers different rotational correlation times for Gd–O and Gd–H rotating vectors (τ_{RO}^{298} and τ_{RH}^{298}, respectively) [48]. For geometrical reasons, their ratio ($\tau_{RH}^{298}/\tau_{RO}^{298}$) has to lie between 0.65 and 1. The most important parameters obtained from the best simultaneous least-squares fit to the experimental data are listed in Table 1. For the complete fitting results, see Table S9.
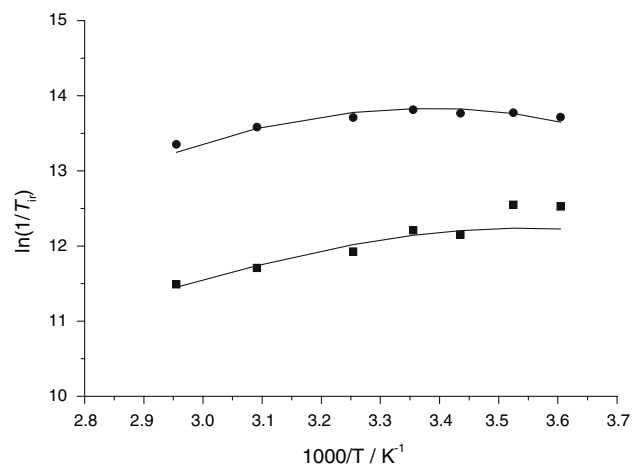
The water exchange of Gd_2L^1 is slightly slower than that found for gadolinium 1,4,7,10-tetraazacyclododecane-1,4,7,10-tetraacetate (GdDOTA) [49]. It is interesting to note that for the monohydrated Gd^{3+} complex of the DO3A ligand bearing an N-linked CH_2CH_2NHCO-pyridyl pendant arm, much faster water exchange has been reported ($k_{ex}^{298} = 1.1 \times 10^8$ s^{-1}) [43]. This fast water exchange has been explained by the steric destabilization of the Ln–water binding interaction by the presence of the bulky substituent. Such a destabilization effect is expected to be less important in Gd_2L^1 since the amide carbonyl is linked to a flexible –CH_2–N– moiety in contrast to the direct attachment to a pyridyl group in the previous case. This limited steric constraint around the water binding site will then be

A

B
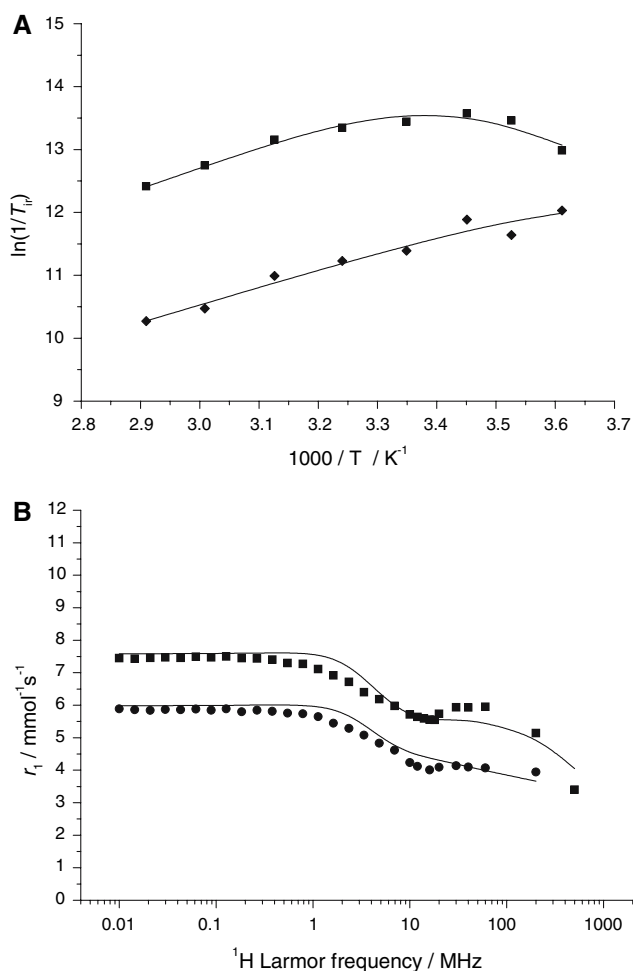
Fig. 6 Variable-temperature ^{17}O NMR [**a**; $\ln(1/T_{1r})$ *diamonds*, $\ln(1/T_{2r})$ *squares*] and ^{1}H nuclear magnetic relaxation dispersion (**b**; 298 K *squares*, 310 K *circles*) data of Gd$_2$L^1 in the absence of Ca^{2+}. The *curves* correspond to the simultaneous fit as explained in the text

Fig. 7 Variable-temperature, reduced longitudinal (*squares*) and transverse (*circles*) ^{17}O relaxation rates for Gd$_2$L^1, in the presence of 1 M Ca^{2+}. The *curves* correspond to the fit as explained in the text

Table 1 Kinetic and structural parameters obtained from the fit of ^{17}O NMR and NMR dispersion (*NMRD*) data for the Gd$_2$L^1 complex in the absence and in the presence of Ca^{2+}, compared with those of gadolinium 1,4,7,10-tetraazacyclododecane-1,4,7,10-tetraacetic acid (*GdDOTA*)

Parameters	Gd$_2$L^1 ^{17}O NMR + NMRD	Gd$_2$L^1 + Ca^{2+} ^{17}O NMR	GdDOTA ^{17}O NMR + NMRD[a]
k_{ex}^{298} (10^6 s^{-1})	2.4 ± 0.2	7.5 ± 1.6	4.1
$\Delta H^{\ddagger}$ (kJ mol^{-1})	43.6 ± 3.3	*43.6*	49.8
$\Delta S^{\ddagger}$ (J mol^{-1} K^{-1})	+23.5	+33.0	–
τ_{RO}^{298} (ps)	350 ± 50	1,150 ± 250	77
E_r (kJ mol^{-1})	24 ± 1	21 ± 6	16.1
τ_v^{298} (ps)	20.6 ± 2.7	0.13 ± 0.02	11
Δ^2 (10^{20} s^{-2})	0.46 ± 0.10	0.50 ± 0.05	0.16
q	*0.4*	*0.7*	*1*
$q^{2\ ns}$	*1*	*1*	–
r_1^{298} (mM^{-1} s^{-1}) 20 MHz	5.74	6.13	4.74

Parameters in *italics* were fixed during the fitting

[a] Reference [49]

translated by a more sluggish water exchange as observed for Gd$_2$L^1. The more than 1 order of magnitude difference in the water exchange rate between Gd$_2$L^1 and the Gd^{3+} complex of the DO3A–CH$_2$CH$_2$NHCO–pyridyl ligand is a good example of the importance of the steric compression around the water binding site. Steric compression is indeed the main factor determining the rate of exchange in a dissociative water exchange mechanism, characteristic of nine-coordinate complexes [50]. The dissociative activation mode for Gd$_2$L^1 is indicated by the positive value of the activation entropy.

The higher τ_r value of Gd$_2$L^1 compared with that of GdDOTA is rationalized by the higher molecular weight and greater rigidity of the molecule. In spite of the slow rotational motion and the presence of a second hydration sphere in the bismacrocyclic system, the relaxivities are only slightly higher than those of GdDOTA, owing to the low hydration number of Gd$_2$L^1 (q = 0.4).

The simultaneous fit of the ^{1}H and ^{17}O relaxation rates also supplies parameters that describe the electron spin relaxation of the Gd^{3+} complexes, such as τ_v, the correlation time for the modulation of the zero field splitting, its activation energy, E_v, and the mean zero field splitting energy, Δ^2. The values obtained for Gd$_2$L^1 are in the usual range for similar complexes [49].

The ^{1}H NMRD and ^{17}O NMR data of the Gd$_2$L^1 system containing Ca^{2+} could not be fitted simultaneously because the conditions for ^{17}O NMR and ^{1}H NMRD samples differed significantly in terms of the ionic strength and viscosity, and also in the Ca^{2+}-to-Gd^{3+} ratio of the samples. Only the ^{17}O $\ln(1/T_{1r})$ and $\ln(1/T_{2r})$ data were analyzed,

and the relaxivities are given in the electronic supplementary material. The ^{17}O relaxation rates were interpreted by using the same set of equations as for the system without Ca^{2+} (Fig. 7). Analogously, the same parameters were fixed in the fit (except for the hydration number, $q = 0.7$, obtained from luminescence studies). The best fitting was obtained with the parameters listed in Tables 1 and S10. On Ca^{2+} addition, the most flagrant change is observed for the rotational correlation time as obtained from the ^{17}O longitudinal relaxation rates ($\tau_R = 350$ compared with 1,150 ps without and with Ca^{2+}, respectively). We attribute this significant increase mainly to the high ionic strength and viscosity of the ^{17}O NMR sample containing 1 M $CaCl_2$, though some rigidification of the molecule on Ca^{2+} is also expected. The water exchange rate triples on Ca^{2+} binding ($k_{ex}^{298} = 2.4 \times 10^6$ compared with 7.5×10^6 s^{-1}). The decreasing negative charge of the Ca^{2+}-bound Gd_2L^1–Ca complex would be rather expected to diminish the exchange rate in a dissociatively activated process. Among other factors that can compensate this effect, the increased steric demand of the central part after Ca^{2+} binding can lead to a steric destabilization of the Ln–water binding interaction. Overall, the relaxivity increase upon Ca^{2+} addition is mainly related to an increase in the hydration number.

Conclusion

With the objective of Ca^{2+} sensing by MRI in the extracellular space, we synthesized two novel bismacrocyclic ligands containing a Ca^{2+}-sensitive BAPTA-bisamide moiety (Scheme 1). Their Gd^{3+} complexes exhibit relaxivities comparable to that of currently used monomeric MRI contrast agents, in accordance with their larger size but lower hydration numbers ($q < 1$). Upon Ca^{2+} addition, the relaxivities of Gd_2L^1 and Gd_2L^2 increase by 15 and 10%, respectively. These changes are likely insufficient for in vivo MRI detection. Gd_2L^1 is practically insensitive towards Mg^{2+}. The apparent association constants for the Ca^{2+} interaction were obtained from the relaxometric titration curves. They are several orders of magnitude lower for our complexes than those determined for BAPTA^{4-} itself or other tetracarboxylate BAPTA^{4-} analogues. The hydration number of Eu_2L^1 was determined from luminescence lifetime measurements in the absence ($q = 0.4$) and presence ($q = 0.7$) of Ca^{2+}. UV–vis measurements confirmed the presence of two coordination environments that we attribute to a monohydrated and a nonhydrated state (Fig. 5). Upon the coordination of Ca^{2+} in the central part of the ligand, the molecule undergoes a conformational change and an acetate arm, originally coordinated to the Ln^{3+} ion, binds to Ca^{2+} and leaves space for the coordination of a water molecule to the lanthanide, which shifts the hydration state towards the more hydrated species.

References

1. Persigehl T, Heindel W, Bremer C (2005) Abdom Imaging 30:342–354
2. Merbach AE, Tóth É (eds) (2001) The chemistry of contrast agents in medical MRI. Wiley, Chichester
3. Aime S, Botta M, Terreno E (2005) Adv Inorg Chem 57:173–237
4. Caravan P, Ellison JJ, McCurry TJ, Lauffer RB (1999) Chem Rev 99:2293–2352
5. Lowe MP, Parker D, Reany O, Aime S, Botta M, Castellano G et al (2001) J Am Chem Soc 123:7601–7609
6. Aime S, Barge A, Delli Castelli D, Fedeli F, Mortillaro A, Nielsen FU et al (2002) Magn Reson Med 47:639–648
7. Zhou J, Lal B, Wilson DA, Laterra J, van Zijl PC (2003) Magn Reson Med 50:1120–1126
8. Aime S, Botta M, Gianolio E, Terreno E (2000) Angew Chem Int Ed Engl 39:747–750
9. Sun PZ, Schoening ZB, Jasanoff A (2003) Magn Reson Med 49:609–614
10. Que EL, Chang CJ (2006) J Am Chem Soc 128:5942–5943
11. Li W, Fraser SE, Meade TJ (1999) J Am Chem Soc 121:1413–1414
12. Hanaoka K, Kikuchi K, Urano Y, Narazaki M, Yokawa T, Sakamoto S et al (2002) Chem Biol 9:1027–1032
13. Aime S, Delli Castelli D, Fedeli F, Terreno E (2002) J Am Chem Soc 124:9364–9365
14. Hanaoka K, Kikuchi K, Urano Y, Nagano T (2001) J Chem Soc Perkin Trans 2 1840–1843
15. Louie AY, Huber MM, Ahrens ET, Rothbacher U, Moats R, Jacobs RE et al (2000) Nat Biotechnol 18:321–325
16. Perez JM, Josephson L, O'Loughlin T, Hogemann D, Weissleder R (2002) Nat Biotechnol 20:816–820
17. Woods M, Zhang S, Ebron VH, Sherry AD (2003) Chem Eur J 9:4634–4640
18. Zech SG, Eldredge HB, Lowe MP, Caravan P (2007) Inorg Chem 46:3576–3584
19. Krause W (ed) (2002) Contrast agents I. Magnetic resonance imaging. Topics in current chemistry, vol 221. Springer, Heidelberg
20. Atanasijevic T, Shusteff M, Fam P, Jasanoff A (2006) Proc Natl Acad Sci USA 103:14707–14712
21. Meldolesi J (1998) Nature 392:863–866
22. Burgoyne RD (2007) Nat Rev Neurosci 8:182–193
23. Tsien RY, Waggoner A (1995) In: Pawley JB (ed) Handbook of biological confocal microscopy, 2nd edn. Plenum, New York, pp 267–280
24. Li W, Parigi G, Fragai M, Luchinat C, Meade TJ (2002) Inorg Chem 41:4018–4024

25. Tsien RY (1980) Biochemistry 19:2396–2404
26. Graeppi N, Powell DH, Laurenzcy G, Zékány L, Merbach AE (1995) Inorg Chim Acta 235:311–326
27. Amman C, Meyer P, Merbach AE (1982) J Magn Reson 46:319–321
28. Raiford DS, Fisk CL, Becker ED (1979) Anal Chem 51:2050–2051
29. Zitha-Bovens E, Vander Elst L, Muller RN, van Bekkum H, Peters JA (2001) Eur J Inorg Chem 12:3101–3105
30. Yerly F (1999) Visualiseur 2.3.4. Institut de Chimie Moléculaire et Biologique, EPFL-BCH, Lausanne
31. Yerly F (1999) Optimiseur 2.3.4. Institut de Chimie Moléculaire et Biologique, EPFL-BCH, Lausanne
32. Wong W, Li C (2005) Int Patent Appl WO 2005003105 A1 20050113
33. Wei W, Tomohiro T, Kodaka M, Okuno H (2000) J Org Chem 65:8979–8987
34. Adam SR, Kao JPY, Grynkiewicz G, Minta A, Tsien RY (1988) J Am Chem Soc 110:3212
35. Corsi DM, Platas C, Van Bekkum H, Peters JA (2001) Magn Res Chem 39:723
36. Horrocks WD Jr, Sudnick DR (1979) J Am Chem Soc 101:334–340
37. Supkowski RM, Horrocks WD Jr (2002) Inorg Chim Acta 340:44–48
38. Beeby A, Clarkson IM, Dickins RS, Faulkner S, Parker D, Royle L, de Sousa AS, Williams JAG, Woods M (1999) J Chem Soc Perkin Trans 2 493–503
39. Albin M, Farber GK, Horrocks WD Jr (1984) Inorg Chem 23:1648–1651
40. Geier G, Jorgensen CK (1971) Chem Phys Lett 9:263–264
41. Tóth É, Ni Dhubghaill OM, Besson G, Helm L, Merbach AE (1999) Magn Res Chem 37:701–708
42. Yerly F, Dunand FA, Tóth É, Figueirinha A, Kovács Z, Sherry AD, Geraldes CFGC, Merbach AE (2000) Eur J Inorg Chem 1001–1006
43. Congreve A, Parker D, Gianolio E, Botta M (2004) Dalton Trans 1441–1445
44. Frey ST, Horrocks WD Jr (1995) Inorg Chim Acta 229:383–390
45. Caravan P (2006) Chem Soc Rev 35:512–523
46. Lebdušková P, Hermann P, Helm L, Tóth É, Kotek J, Binnemans K, Rudovský J, Lukeš I, Merbach AE (2007) Dalton Trans 493–501
47. Lebdušková P, Sour A, Helm L, Tóth É, Kotek J, Lukeš I, Merbach AE (2006) Dalton Trans 3399–3406
48. Dunand FA, Borel A, Merbach AE (2002) J Am Chem Soc 124:710–716
49. Powell DH, Dhubhghaill OMN, Pubanz D, Helm L, Lebedev YS, Schlaepfer W, Merbach AE (1996) J Am Chem Soc 118:9333–9346
50. Laus S, Ruloff R, Tóth É, Merbach AE (2003) Chem Eur J 9:3555